

Weight Reduction Methodologies for Wave Energy Devices: A Structural Analysis Approach

R. Sharvin, M. O'Shea

Abstract— The floating Backward Bent Duct (BDD) Buoy oscillating water column model generates electricity through the fluctuation in wave height. Wave energy conversion devices are often faced with a particularly high levelized cost of energy (LCOE) when compared to other renewable energy devices, and various investigations into bridging this gap have been carried out in recent history. Previous studies on the BDD Buoy have suggested that a significant reduction in required construction material is possible as a result of reduced differential pressures acting across the hull walls in operational conditions. Various structural analysis campaigns have been conducted on sections of the hull to assess this theory.

A Finite Element Analysis (FEA) was performed on a full-scale model of the BDD Buoy under extreme design wave loadings in based on wave data at EMEC's Billia Croo test facility in Orkney, Scotland using Robot Structural Analysis software. A maximum pressure of 145 kPa was calculated for an 18.7 m peak wave height at Billia Croo. The BDD Buoy was modelled for both static and dynamic load conditions under various constraint layouts. A modal analysis was conducted on the model which estimates the natural frequency of the BDD Buoy to be approximately 6.67 Hz.

Keywords—FEA, LCOE, Modal Analysis, Natural Frequency, Resonance, WEC

Part of a special issue for EWTEC 2023. Original version published in EWTEC 2023 proceedings at <https://doi.org/10.36688/ewtec-2023-661>. Manuscript submitted 9 September 2024; Accepted 4 February 2025. Published 31 May 2025

This is an open access article distributed under the terms of the Creative Commons Attribution 4.0 International license. CC BY <https://creativecommons.org/licenses/by/4.0/>. Unrestricted use (including commercial), distribution and reproduction is permitted provided that credit is given to the original author(s) of the work, including a URI or hyperlink to the work, this public license and a copy right notice.

This article has been subjected to single-blind peer review by a minimum of two reviewers.

R. Sharvin is with the Department of Civil, Structural & Environmental Engineering, University College Cork, Cork, Ireland (e-mail: rorysharv@outlook.com).

M. O'Shea is with the Department of Civil, Structural & Environmental Engineering, University College Cork, Cork, Ireland (e-mail: michaeloshea@ucc.ie).

Digital Object Identifier: <https://doi.org/10.36688/imej.8.1-11>

I. INTRODUCTION

A. Overview

THE BDD Buoy was initiated with the intention of developing and commercialising a wave energy converter that provides a clean and consistent renewable source of energy at a competitive cost alongside other renewable energy sources such as solar and wind. The device is based on the Backward Bent Duct Buoy oscillating water column wave energy converter design, originally invented by Yoshio Masuda in the 1980s [1], which employs the fluctuation in wave height to compress air in a water column, forcing it through a turbine and thus generating electricity.

The importance of renewable energy cannot be overstated, as it represents a critical component of the effort to address climate change and reduce our reliance on fossil fuels. Offshore renewables, in particular, have the potential to play a significant role in this transition. Unlike onshore renewable energy sources, offshore renewables, such as wind, wave, and tidal power, can offer a more consistent and reliable source of energy due to the stronger and more consistent wind and water currents present offshore. Additionally, offshore renewable energy development can help to alleviate some of the pressure on overburdened onshore energy infrastructure while providing new opportunities for job creation and economic development in coastal communities.

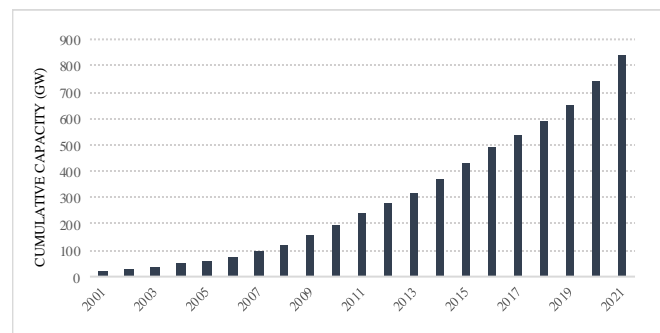


Fig. 1 Global cumulative installed wind power capacity 2001 – 2021 [2]. Exponential increase over the last 20 years with pattern projected to continue.

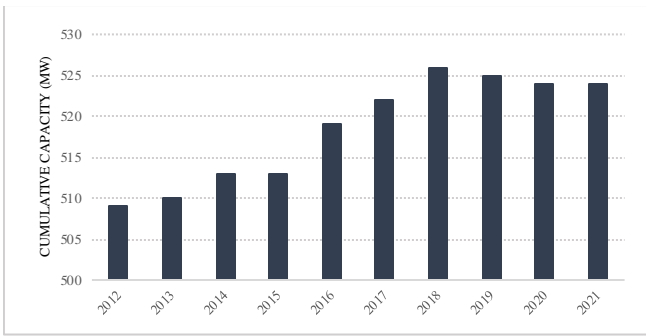


Fig. 2 Global cumulative installed marine power capacity 2012 – 2021 [4]. Plateau in recent years reflects a lack of effort to capitalise on the massive potential of marine energy.

1) Wave Energy and the Energy Market

The offshore renewable energy market is dominated primarily by wind. Wind energy is one of the world's fastest growing energy sources, with the global cumulative capacity of installed wind energy approximated at 745 GW as of 2021, with this figure projected to reach 840.9GW by the end of 2022 [2]. In recent years, the global offshore wind market has become one of the most lucrative and fastest growing markets in the world and is expected to grow from an estimated USD 77.77 billion in 2021 to USD 174.75 billion by 2030 [3]. In contrast, as of 2021 the global cumulative capacity of installed wave and tidal energy was reportedly approximately 524 MW [4], unchanged from the previous year. The global wave and tidal energy market size for 2021 was valued at approximately USD 0.59 billion to USD 4.41 billion by 2028 [5].

2) Wave Energy in the Renewables Sector

Wave energy technologies have not been widely used for utility-scale power supply because of their high manufacturing and maintenance costs compared to other renewable technologies. Wave energy converters are designed to resist heavy loading from wave impacts, which drives up the Levelized Cost of Energy (LCOE) of manufacturing such devices. The current design for the leading commercial scale BBD Buoy weighs approximately 800 tonnes and has the capacity to generate 1.25 MW of electricity from harnessed wave energy. [1] compares the cost-effectiveness of the BBD Buoy against various offshore renewable energy devices with regards to the power capacity to weight ratio of each device, illustrating the significantly greater efficiency of current wind turbines in this respect when compared to the BBD Buoy.

TABLE I
EFFICIENCY OF BBD BUOY VS OFFSHORE WIND TURBINES [11], [12], [13]

Energy Device	Capacity (MW)	Weight (t)	Capacity:Weight (kW/t)
BBD Buoy	1.25	826	1.513
Rampion V112-3.45MW Offshore Wind Turbine	3.45	366	9.426
Siemens SWT-3.60-120 Offshore Wind Turbine	3.6	475	7.579
Siemens SWT-6.0-154 Offshore Wind Turbine	7	970	7.216
Vestas V164-8.0MW Offshore Wind Turbine	8	855	9.357
Siemens Gamesa SG 14-222 DD Offshore Wind Turbine	14	1200	11.667

The high LCOE of wave-generated electricity is the leading factor hindering the widespread commercial development of wave energy devices and places the BBD Buoy in a particularly unfavourable position in terms of power generation per unit weight when compared to wind-generated energy. Previous studies on wave energy converters have explored methods of improving the efficiency of the BBD Buoy to achieve a more market-competitive design to rival the power production efficiency of competitor offshore renewable energy devices. To achieve this, a significant amount of weight would need to be removed from the existing design by reducing the amount of material used in construction. The feasibility of adapting such a revised design is a principal goal of this study. An FEA conducted on the full-scale BBD Buoy would provide a greater understanding of the behaviour of the current design under operational loadings and how this behaviour would change by adapting a more lightweight hull design using either lighter materials or reduced thickness.

B. Results of Previous Model Testing

BBD OWC models have undergone testing at various scales to achieve optimal performance. Trials conducted at HMRC at a 1:50 scale determined the optimised configuration that could be applied to the 1:15 model tested at ECN, Nantes (University College Cork, 2005) and later at University College Cork's Lir National Ocean Test Facility (NOTF) in 2021 [6]. A 1:15 model built with steel would have required a thickness of less than a millimetre, thus glass-reinforced plastic was selected for construction. The main objective was to examine the possibility of reducing the hull thickness to lower manufacturing costs of the buoy and wave energy converters in general.

The 2021 study at the National Ocean Test Facility revealed that the differential pressure across the hull

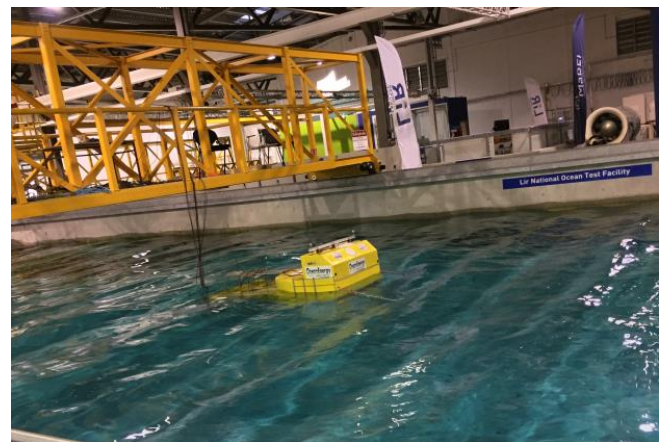


Fig. 3 Testing of 1:15 BBD Buoy model at Lir NOTF [6].

walls was 15-28% of the magnitude of the total hydrostatic pressures, suggesting that a lightweight open hull design may be feasible [6]. A structural analysis using Ansys consequently estimated that a 60% reduction in hull weight was possible using these reduced

pressures. This study will carry out a Finite Element Analysis on the entirety of the full-scale structure utilising operational wave pressure data collected from previous investigations such as the 1:50 model testing to provide a more conclusive outlook on the feasibility of such a weight reduction.

C. Alternate Materials for Hull Construction

superior mechanical properties. E-glass and S-glass fibre cloths boast very favourable mechanical properties and are considerably lighter materials than steel. They are composed of glass, not carbon and as such have a 0% carbon content, however the production of glass fibres requires a significant amount of energy.

D. Gap in the State of the Art

TABLE II
MATERIAL PROPERTIES [15], [16], [23]

Material	Young's Modulus (GPa)	Ultimate Tensile Strength (MPa)	Yield Strength (MPa)	Density (kg/m ³)	Cost (€/kg)	Carbon Content (%)
Grade A/S235JO Steel	210	360 - 510	235	7850	1.50 - 2.00	0.17
Aluminium Alloys						
5000 Series	68 - 73	180 - 386	80 - 214	2660 - 2680	2.00 - 3.00	0.5 - 6
6000 Series	68 - 73	130 - 310	60 - 260	2700 - 2710	1.80 - 2.50	<0.1
Fibreglass						
E-Glass	70 - 80	200 - 400	150 - 300	2550 - 2600	2.00 - 10.00	0
S-Glass	85 - 95	1500 - 2500	1000 - 1500	2490 - 2550	8.00 - 40.00	0
Carbon Fiber	100 - 300	1000 - 3000	500 - 2000	1750 - 1800	20.00 - 100.00	>90
Aramid Fibres						
Kevlar 29	70 - 131	2400 - 3600	2100 - 2400	1440	45.00 - 95.00	58
Kevlar KM2	131 - 153	3300 - 3700	2700 - 3100	1440	75.00 - 140.00	58
Kevlar 49	131 - 145	3600 - 3800	3400	1440	90.00 - 185.00	65

Marine vessels and infrastructure in the size range of the latest commercial BBD Buoy require conventional building materials such as steel for their extensive workability and machinability in construction, as well as requiring a strong enough material to withstand the significant loadings to which the structure will be subjected by the surrounding environments. The current design for BBD Buoy employs primarily Grade A/S235JO Steel for the hull and adjoining members, resulting in a relatively heavy structure [7]. Considering more lightweight materials as an alternative would aid in addressing this issue, but factors such as cost, embodied carbon, availability, and ease of manufacturing must be considered during the selection process. These factors will influence the feasibility and economic viability of a revised design that uses alternative materials while sustaining the necessary mechanical properties to maintain structural integrity.

Table II summarises each of the materials selected for consideration and compares the key mechanical properties with one another, along with the densities, per-weight costs, and typical carbon content of each. It is worth noting that the more specialised fibreglass cloths like carbon fibre, aramid fibre cloths, and composite derivative materials are most commonly used in high performance marine applications in which strength-to-weight ratios are prioritised over key factors considered in this study like cost and carbon footprint.

Carbon fibre along with the aramid fibres have a high carbon content and are significantly more expensive than the other alternatives. As a result, it was decided not to pursue these materials in the FEA campaign despite their

1) Unlocking the Potential of Wave Energy

The theoretical resource capacity of ocean waves is capable of meeting 100% to 400% of the world's electricity needs as of 2020 [8]. However, the current capacity of installed marine energy is only 532 MW, with over 98% represented by tidal technology, suggesting we are not unlocking the ocean's full potential as an energy source. The theoretical electricity generation potential of tidal energy is the lowest of all ocean energy technologies, at around 1,200 TWh/yr, largely due to limited site availability and high capital investment [9]. In contrast, the theoretical electricity generation potential of wave energy is estimated to be around 29,500 TWh/yr, which has the capacity to meet all global energy demands [8]. Wave energy has an advantage over wind and solar as a source of renewable energy because it offers stability to the grid and provides flexibility to the energy system. Wave energy is still in a relatively experimental phase, and technologies have not converged towards one particular design, with ten different designs currently being pursued worldwide. Should a significant refinement in design be reached for a specific wave energy converter such that the potential for mass production could be met, ocean energy could ultimately play a key role in the solution to the global energy crisis.

The results of the studies conducted at the Lir NOTF suggest that the commercialisation of wave energy devices is close. Further investigation into a thinner hull design or more lightweight alternatives to steel could lead to achieving a reduced LCOE of the BBD Buoy and wave energy devices as a whole. These studies however

did not consider the impact of dynamic loading or the fatigue limit state, which are crucial aspects in understanding the behaviour of the structure and the consequent effects of a weight reduction. While Robot Structural Analysis software does not have the capabilities to perform an assessment of fatigue limit states, the modal analysis conducted in this FEA campaign is a significant step forward providing valuable information on the Buoy's behaviour under dynamic loading.

2) Wave Slamming

The total forces acting on a structure due to a wave impact can be divided into the quasi-static force (Morison force) and the slamming force due to breaking waves. The wave slamming forces are very large forces acting for a short period of time. The initial impact induces a high frequency response in the structure. Fig. 4 indicates such a response in a truss subject to a wave slamming force. In this instance, the impact duration is considerably small, however impact durations can range anywhere from 0.02 – 0.2 seconds. Should the natural frequency of the device reside within this range there is a possibility that a wave slam event could induce resonance with the structure.

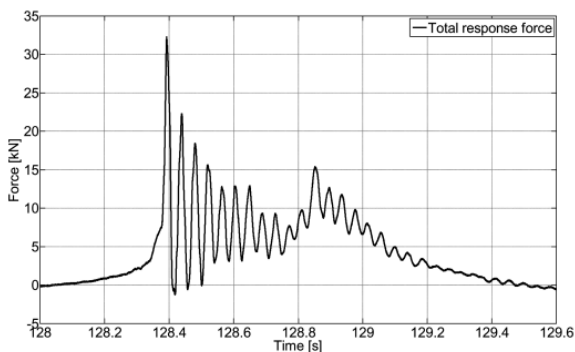


Fig. 4 Response of truss structure to wave slamming [18].

Objectives of Research

The objectives of the experiment and analysis detailed in this study were:

- 1) Modelled maximum design wave pressures for a peak 18.7 m wave height recorded at Billia Croo.
- 2) To perform a FEA on a full-scale model of the BBD Buoy applying the operational wave pressures for testing in Hawaii (moderate) and in Orkney, Scotland (extreme), for both static and dynamic loading.
- 3) To assess any key areas of concern in the current design which arise as a result of the Finite Element Analysis of the static and in particular the dynamic loading on the BBD Buoy.
- 4) To assess the effects of introducing alternate materials to the design on the behaviour of the structure.

The FEA of the dynamic behaviour of the full-scale BBD Buoy carried out in this study is a novel area in the lifespan of the device and floating open-hull structures in general, and as such could potentially yield previously unforeseen results. The FEA conducted in this study was based on the findings for operational loadings in previous deployment scale BBD Buoy designed for moderate sea states in Hawaii and scale physical modelling at the Lir National Ocean Test Facility [6], and modelled for the loading conditions expected during testing at extreme conditions in Scotland.

II. MATERIALS AND METHODS

A. FEA Model

The FEA model of the BBD Buoy was developed in Robot Structural Analysis, shown in Fig. 5. The model employed a hull thickness of 12 mm, with Rectangular Hollow Sections (RHS) comprising the primary framing. All purlins and stiffeners were taken as 5" x 3.5" x 0.375" L-Sections. All modelled elements were assigned material S235 structural steel, with a yield strength of 235 MPa and an allowable stress of 141 MPa. Walkways, fenders, and the surrounding structure of the turbine were omitted from the Finite Element Model, and a preliminary design was assumed for the canopy top to simplify the analysis and ensure more consistent calculations and results were

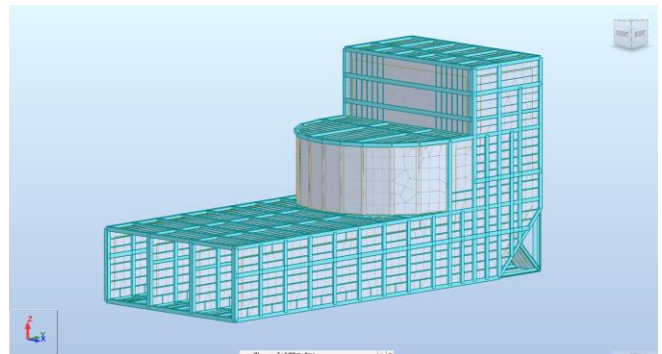


Fig. 5 BBD Buoy Finite Element Model. All panels and members S235 steel.

produced by Robot.

Despite the omission of the aforementioned structural elements, the FEA model is a considerably large structure for Robot to analyse. As such, the FE meshing generated for the model needed to be optimised for accurate and reliable results, while avoiding an accumulation of errors stemming from overly cumbersome calculations. An element sensitivity study was therefore undertaken to assess the influence of the mesh element size and type on the accuracy and reliability of the simulation results. A square meshing was deemed most suitable due to the geometry of the structure. Mesh size varied from 0.75 m, 1.00 m, and 2.00 m in length to assess their impact on the overall model response. As the mesh size was reduced and the overall meshing became more refined, the results began to converge. The optimal mesh density was found to be 1.00 m elements, as from here the values of the

maximum stresses began to plateau. The results for the 1.00 m and 0.75 m results were considerably similar, while the former consisted of 2,000 less nodes than the latter. The 1.00 m mesh selected used 4610 nodes and resulted in less cumbersome calculations while still producing accurate and reliable results.

B. Model Constraints

1) *3-2-1 Constraint System*

The standard practice modelling BBD Buoy restraints is to use a 3-2-1 constraint system to represent the movements of a structure in three-dimensional space. This system involves constraining certain degrees of freedom while leaving others free. The system is based on the idea that a structure can move in six degrees of freedom, and it is not always necessary to model all of them. The Robot model and Ansys model shown in Fig. 6 both employ the 3-2-1 constraint system, with the support at point 1 in both models constrained in all three directions of freedom. However, the X and Y axes are flipped in the Robot model, with point 2 constrained translationally in the Y and Z axes and point 3

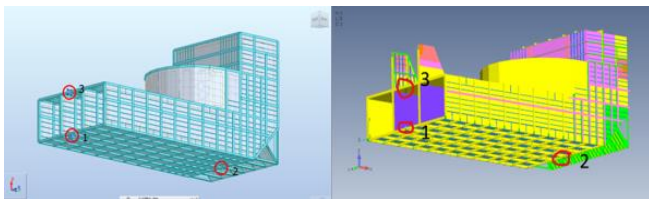


Fig. 6 3-2-1 constraint systems for Robot model.

constrained translationally in only the Y axis.

2) *Mooring Constraints*

The support system of the BBD Buoy during operation will behave differently from the 3-2-1 constraints modelled, so FEA was carried out for different support layouts to account for this. The device will effectively be supported vertically by water and laterally by the use of a mooring system at the bow and stern of the structure, illustrated in Fig. 7. The device is currently constrained by a three-point mooring system; however, a four-point bridle mooring system was also analysed as a potential alternative. The mooring lines extend horizontally from the hull to the mooring buoy.

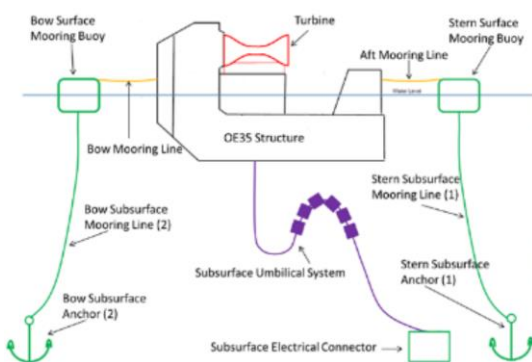


Fig. 7 BBD Buoy mooring layout [19]

The supports applied to the model were restrained in the x and/or y directions only at these points to replicate the mooring constraints. In actuality, the bow constraint(s) likely would not support the structure during wave impacts to the rear, and would instead only constrain the model laterally in the x direction, i.e., for side-on wave impacts, with the stern moorings constraining the model in the y. To account for this, two models were analysed for each mooring system layout, one constraining all mooring points in the x and y directions and another constraining the model in the x and y direction at the stern moorings and constraining the bow mooring(s) in the x direction only (point 1 for the three-point model and points 1 and 2 for the four-point model in Fig. 8).

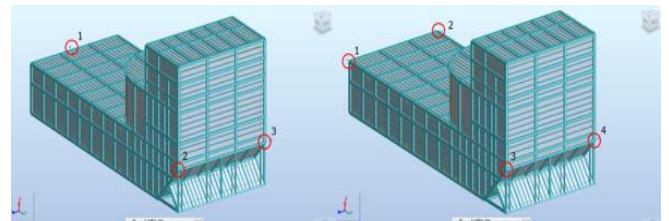


Fig. 8 Three-point and four-point mooring support layouts.

C. Loading Conditions

This study examined specifically operational wave pressures in Hawaii (moderate) and peak wave loadings in Orkney, Scotland (extreme) on the BBD Buoy. Four equations of wave pressure were considered to calculate the wave loading on the Buoy in the environmental conditions expected during the testing at the Billia Croo test berth. The test berth is located roughly 2km offshore at an assumed depth of 60 m, with maximum wave heights recorded of up to 18.7 m [10]. Wave pressures were calculated for impacts to both the rear of the device and to the side of the structure. Fig. 9 illustrates the variation in calculated wave pressures for each design formula with the respective values tabulated in Table III.

While Goda’s Pressure Distribution yielded the highest

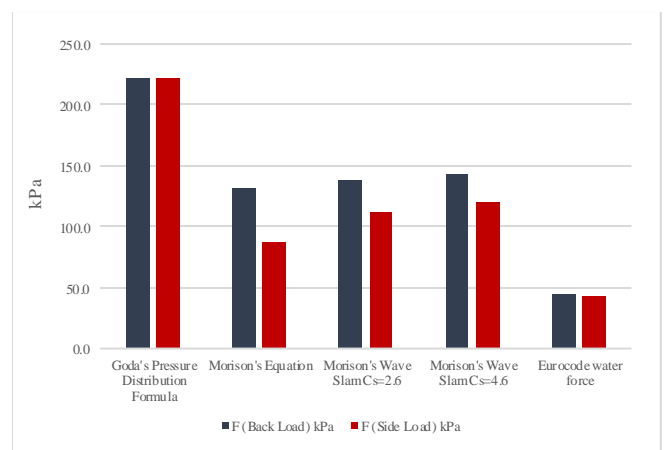


Fig. 9 Wave pressures for Extreme load case.

wave pressures of approximately 221.9 kPa, Morison's equation and Morison's wave slam were deemed more appropriate for the operational conditions of the device considered in this study, as both Morison's equation and wave slam take the effects of the inertial and drag forces of the water on the structure into account. Static lateral pressures were applied to the rear and side of the model, shown in Fig. 10.

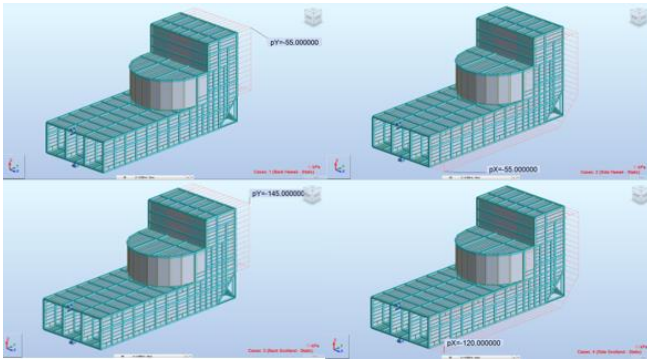


Fig. 10 Extreme (top) and Moderate (bottom) load cases for 3-2-1 constrained model.

D. Modal Analysis

1) Modal Analysis of BBD Buoy FEA Model

The modal analysis for the BBD Buoy was generated in Robot Structural Analysis to calculate 20 modes at a tolerance of 0.0001 with 40 iterations. This was carried out for the 3-2-1 constraint model and the three-point mooring model constrained at the bow in the x-direction. The 3-2-1 constraint and three-point mooring models were assumed to best replicate the behaviour of the BBD Buoy in operational conditions, and as such the critical modes observed will likely occur at frequencies most comparable with the natural frequency of the actual device. Through this analysis, various critical frequencies could be identified at which the structure is most susceptible to wave loads. An assessment of each mode shape was then carried out to locate areas of particular vulnerability and the corresponding frequencies at which extreme deformations were occurring.

2) Alternate Material Models

The FEA of the Buoy ruled out several alternative materials due to extreme stresses and economic viability. Peak stresses identified in the static loading analysis surpassed the allowable limit of the aluminium alloys considered. Aramid and carbon fibres were eliminated as options due to their high cost-per-weight, while E-glass and S-glass reinforced fibre cloths were found to possess similar mechanical qualities to Grade A/S235JO Steel while maintaining competitive prices. Models utilising a combination of steel and S-glass were constructed and subjected to static loading and modal analysis. The key objective was to note any variation in the natural frequencies and critical modes of each model as a result of the introduction of the new materials. The study only

considered alternative materials for the construction of the hull and not for structural members.

3) Corrected Self-Weight Models

The omission of key elements of the design in the Finite Element Model (walkways, fenders, canopy, etc.) resulted in a considerably lower model self-weight of 570 tons when compared to the structure's true weight of approximately 826 tons. Self-weight was negated from the modal and static analyses of the original steel and alternate material models as the weight of the structure could effectively be assumed to be supported by buoyancy forces. This approach provided a more accurate representation of the operational constraint conditions by allowing the supports to act in the x and y axes only and not have to support the structure self-weight which is effectively supported by buoyancy forces. However, negating the self-weight of the structure entirely may lead to some inaccuracies in critical mode shapes and natural frequencies. A modal analysis was thus carried out for a Load to Mass conversion of the self-weighted model using a factor of 1.45, resulting in a corrected self-weight of 826.5 tons. The modes from this analysis could then be compared with the critical frequencies obtained in the modal analysis of the floatation supported models to verify the reliability of the results.

4) Turbine Models

The intent of analysing the corrected self-weight models was to account for the loss of mass in the verification of the natural frequencies, however in these instances the negated mass is effectively assumed to be distributed evenly throughout the model in these analyses. This is not in fact the case, and one of the major components neglected in the model was the turbine, located above the plant room. The turbine is a considerably heavy component with its weight concentrated around a much smaller area, and thus when compared to the corrected self-weight models could have a significantly larger effect on the mode shapes and critical frequencies than when the negated weight is distributed evenly throughout the model. A modal analysis was carried out on the 3-2-1 constraint and the three-point mooring models with a Load to Mass

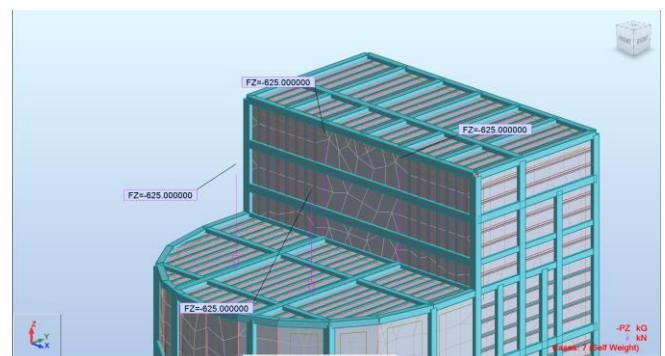


Fig. 11 Turbine loads on model.

conversion of the turbine loads comprising the negated weight of the Buoy, illustrated in Fig. 11.

E. Harmonic Loading

The structure was subjected to harmonic loading at various critical frequencies identified from the modal analysis. Fig. 12 shows the deformed shape of the model and the corresponding harmonic loading applied. The study investigated the effects of various wave impacts on the stresses within the structure which could induce resonance and cause excessive vibrations. Loadings were

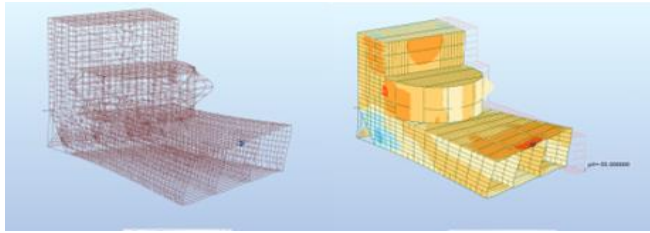


Fig. 12 Harmonic loading applied at critical frequencies.

also applied to the model at frequencies which were more representative of the expected waves to replicate the kind of dynamic loading anticipated from wave impacts. Taking a typical average wave period of 20 seconds, both the base wave loading, and the peak design wave loadings were applied at a frequency of 0.05 Hz.

III. RESULTS

A. Wave Pressures

A summary of all wave pressures calculated are included in Table III for both load cases. The values calculated for Morison’s wave slam taking Cs as 4.6 were taken for as design loads. As the moderate load case was modelled as the base wave loading, a pressure of 55 kPa was taken for both the back and side pressures. The Extreme load case was considered as the design load case and as such wave loadings corresponding to the affected

areas of 145 kPa and 120 kPa were taken for back and side loading, respectively.

B. FEA of Static Loading

The FEA found a consistent development of localised stress points at constraints across all models under each load condition. In all cases the localised stress points yielded peak stresses above the allowable 141 MPa limit of Grade A/S235JO steel. Table IV and Table V arrange the peak stresses with their corresponding locations under back and side loading, respectively, for each model. The 3-2-1 constraint layout is based off the commercial BBD Buoy model and, while it does not replicate the actual constraint behaviour of the BBD Buoy, it does effectively act as a control model to which the

TABLE III
SUMMARY OF WAVE LOADING

Formula	F (Back Load) kPa	F (Side Load) kPa
Goda's Pressure Distribution Formula	221.9	221.9
Morison's Equation	132.1	88.7
Morison's Wave Slam Cs=2.6	138.4	113.6
Morison's Wave Slam Cs=4.6	143.2	118.5
Eurocode water force	75.3	42.2

results of the mooring-supported models can be compared.

The x-only bow constraints best replicated the mooring supports under back loading as, in operation, the bow mooring would not support the model in the direction of the load in the event of wave impacts from the rear. The peak stresses observed in these models occurred at localised stress points at the apex of the curved plant room wall, indicated in Fig. 13. Although the 3-2-1 constraint model did not replicate the stress distribution under back loading particularly accurately, it provided a good representation of the stresses induced by side-on impacts, with maximum localised stresses occurring at the supports in side loading cases.

The x-only bow constrained four-point model did not

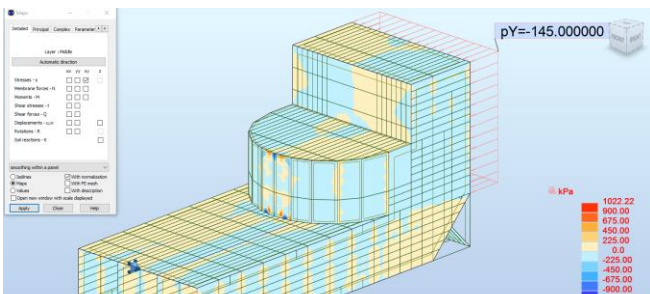


TABLE IV
PEAK STRESS FROM BACK LOADING

Location	Extreme LC Peak Stress (MPa)		Location
	Steel	Composite	
Point 1 (bow)	381.6	381.7	

TABLE V
LOCALISED STRESSES FROM SIDE LOADING

Model	Moderate LC Peak Stress (MPa)		Extreme LC Peak Stress (MPa)		Location
	Steel	Composite	Steel	Composite	
3-2-1 Constraint Layout	363.9	277.1	801.9	604.5	Point 3 (bow)
Three-Point Mooring Model					
X-Y Bow Constraint	354.2	-	772.9	-	Bow and Stern
X-Bow Constraint	354.2	273.4	772.9	590.7	Bow and Stern
Four-Point Bridle Mooring Model					
X-Y Bow Constraint	261.0	-	563.8	-	Bow
X-Bow Constraint	332.5	-	718.2	-	Stern

exhibit the significant improvement of stress distribution which was expected in either back or side loading. However, the bow supports in a four-point bridle mooring system would likely constrain the model in both the x and the y direction in the case of a side-on wave impact. Following this, the x-y bow constrained model experienced considerably lower peak localised stresses than the three-point mooring model in side loading, thus there is potential to better distribute the stresses induced by side-on wave impacts should such a system be utilised.

Peak localised stresses exceeded the design resistances of both aluminium alloys, as well as that of E-glass fibre cloths, therefore only S-glass was modelled as a potential alternative. Two models were developed using S-glass fibre panels with a design resistance of 1667 MPa in place of all S235 steel panels which experienced extreme stresses that surpassed their allowable limit, illustrated in Fig. 14. In actuality, the use of S-glass would only be necessary in areas of localised stresses, however the limited scope of this FEA campaign prohibited the design of such specialised reinforcement.

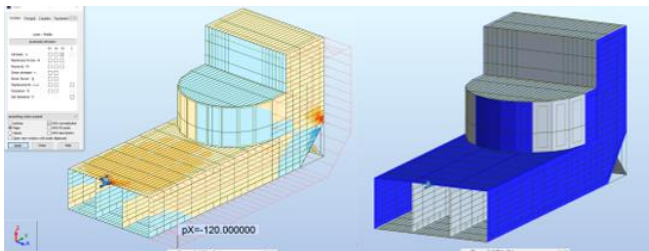


Fig. 14 Localised stress in three-point mooring model and location of S-Glass fibre panels.

Localised stress points in the S-glass fibre cloths experienced approximately a 25% decrease in maximum stresses overall compared to the steel hull. The S-glass model displayed an improved distribution of stress throughout the hull compared to the localised concentrations of stress points in the steel model, which is illustrated in Fig. 15. The composite models averted failure under both load conditions.

C. Modal Analysis and Harmonic Loading

The modal analysis conducted on the steel models identified critical frequencies that could cause resonance and potential failure in the buoy when impacted by

waves with the same frequency as its natural frequency. The extreme winds and harsh wave conditions in the EMEC test berths increase the likelihood of such low-period, high-frequency waves inducing dynamic loading on the buoy. The 3-2-1 constraint and three-point mooring models were used for the analysis.

The 3-2-1 model exhibited severe deformations at lower frequencies than the three-point mooring model.

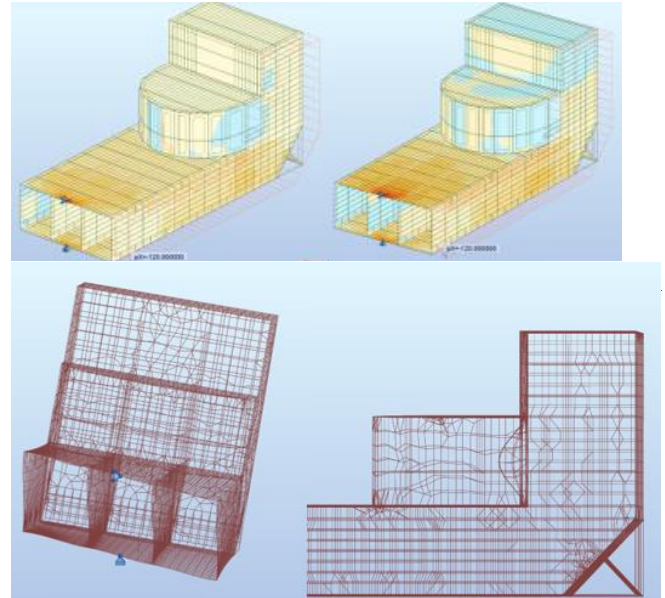


Fig. 16 First critical mode of 3-2-1 model and three-point mooring model.

As illustrated in Fig. 16 below, first signs of significant deformation occurred at 1.40 Hz and 3.43 Hz in the 3-2-1 and three-point mooring model, respectively. The extreme deformation of the 3-2-1 model at such a low frequency is likely due to the constraint layout allowing greater freedom of deformation, with all supports confining in the same z-plane.

At certain frequencies, the deformation was consistent between both models, particularly in the back wall of the plant room, indicating critical modes of concern. The models were subjected to harmonic loading at critical frequencies identified by the modal analysis, shown in Fig. 17, with peak localised stresses of up to 65 GPa observed in the three-point mooring model at a frequency of 6.67 Hz, similar to the 1.40 Hz mode in the 3-2-1 model.

1) Alternate Material Models

The modal analysis for the composite models identified critical modes at similar frequencies to the original steel models. The first critical mode observed in the 3-2-1 composite model occurred at 1.38 Hz, with far higher stresses induced by harmonic loading at this frequency compared to the steel model at its first critical frequency. The three-point mooring composite model exhibited better performance when subjected to lower frequencies with the introduction of S-glass. At 6.60 Hz, the composite model exhibited similar extreme deformation throughout the entire structure as seen in the original steel three-point mooring model at its natural frequency,

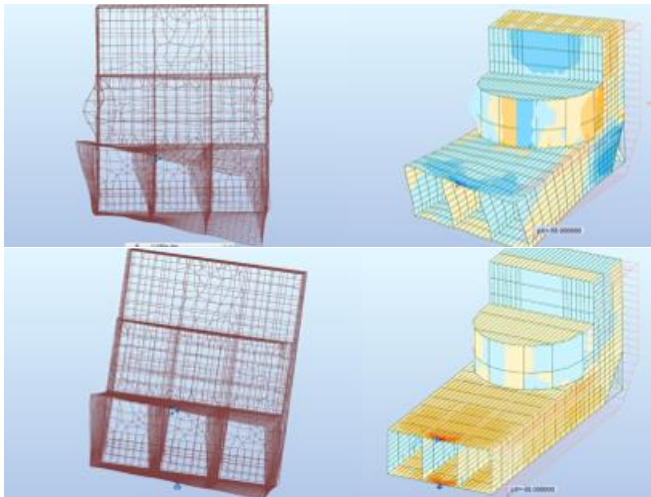


Fig. 17 Harmonic loading of three-point mooring model at 6.67 Hz and 3-2-1 S-Glass/steel model at 1.38 Hz.

but lower maximum stresses at localised stress points were induced compared to the composite model.

2) Verification of Natural Frequencies

The critical modes from the modal analysis of the corrected self-weight model were compared with those observed in the 3-2-1 model which neglected self-weight. The majority of the critical deformations coincided with their zero self-weight counterparts, which suggests that the critical modes of the device identified by the modal analysis can be assumed to be accurate. The natural frequencies of each model are included in Table VI.

3) Turbine Models

The turbine models reached critical modes at lower frequencies than the original and corrected self-weight models as a result of the more inconsistent distribution of mass throughout the structure. The 3-2-1 constraint model reached its first critical mode shape at 0.86 Hz with the turbine load applied, compared to 1.40 Hz in the original model, while the first critical mode occurred at 4.96 Hz in three-point mooring turbine model, compared to 6.67 Hz in the original. When the turbine models were subjected to harmonic loading at these frequencies, peak stresses of up to 48 GPa were observed, presumably resonance-induced, indicating the structure was oscillating at its natural frequency. The modal analysis also identified a second critical mode shape in the 3-2-1 constrained turbine model at 6.18 Hz, however in this

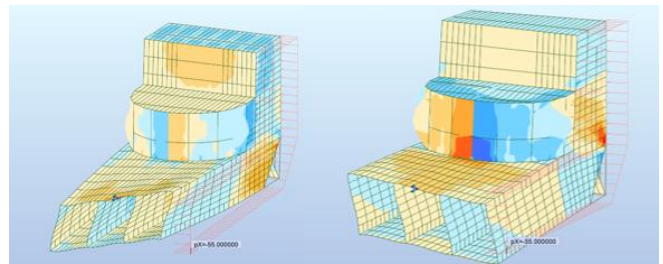


Fig. 18 Resonance in three-point mooring model at 6.67 Hz and in turbine model at 4.96 Hz.

TABLE VI
MODEL NATURAL FREQUENCIES

Model	Natural Frequency (Hz)
3-2-1 Constraint Model	
Steel Model	1.40
Composite Model	1.38
Turbine Model	0.86, 4.49
Three-Point Mooring Model	
Steel Model	6.67
Composite Model	6.60
Turbine Model	6.18

instance resonance was only observed when harmonic loading was applied to the rear of the structure.

4) FEA of Expected Operational Dynamic Loading

The results of the dynamic loading applied at 0.05 Hz representing a typical 20 second period wave found that the steel and composite models exhibited comparable results to the static loads for the base moderate loading, but considerable increases in maximum stress concentrations were observed for the Extreme load case. In the case of the three-point mooring model, a natural frequency of 6.67 Hz would return a period of 0.15 seconds, which lies within the estimated impact duration range for a wave slamming event. It is possible that a wave slam event could induce resonance in the structure and cause severe failure should the true natural frequency of the BBD Buoy under a three-point mooring support layout be comparable with that calculated in this study.

IV. CONCLUSIONS AND RECOMMENDATIONS

A. Conclusions

Various forms of structural analysis have been carried out on the BBD Buoy and other wave energy converters to date, however an analysis in both static and dynamic load conditions on a model of this scale has not been possible in previous studies. The results of this study serve as a significant step forward towards achieving the best conclusive design to optimise the LCOE of mass-producing the BBD Buoy. While some objectives were met with shortcomings, there are a number of key takeaways from this study moving forward:

- While the 3-2-1 constraint model did not replicate the constraint behaviour of the Buoy in operation, the stresses observed at the constraints as well as the distribution of stress throughout the hull was a good representation of the behaviour of mooring supported models.
- When modelling back loading on the three-point mooring supported Buoy in FEA, the bow constraints should be released in the direction of the load to best replicate the behaviour of the mooring system.
- Back loading of the device under mooring constraints induced significant localised stress points at the front of the curved plant room wall. This was consistent for both mooring support layouts.
- The four-point mooring system provided better distribution of stress in the system, as well as yielding considerably lower peak stresses at constraints than the three-point mooring system.
- The models employing a composite S-glass/S235 steel hull displayed no significant change in maximum stresses or distribution of stress during back loading, however exhibited a 25% reduction in maximum stress and an improved distribution of stress during side loading.
- The models developed in this study yielded localised stresses which would have induced failure in the alternative lightweight materials. The limitations of the modelling software meant that these materials could not be employed in less stress-concentrated regions away from localised stress points, however the use of these lighter alternatives may be possible through further analysis by reinforcing localised stress points.
- The results of the modal analysis found that in a three-point mooring support layout the natural frequency of the BBD Buoy is likely to reside around 6.67 Hz, which results in a period of 0.15 s. It is possible that a wave slam event could have an impact duration of this length and induce resonance, causing extreme stress and deformation.
- Conduct FEA using Ansys or a similarly capable FEA software including stiffeners and other specialised reinforcement to localised stress points at the mooring supports and particularly the plant room front wall under back loading. The results of the modal analysis suggest that the back wall of the plant room was the first area to exhibit significant deformation at low frequencies. It is recommended that further analysis be carried out with particular attention paid to the localised stress points identified from the back loadings, and that reinforcement to both plant room walls is considered.
- Investigate further a potential four-point bridle mooring support system for the BBD Buoy. The mooring supports could be located at the proposed lifting points and serve a dual purpose, which would reduce the overall required reinforcement and in turn lower the LCOE.
- Further investigation should be undertaken into the expected impact durations of a wave slam for the environmental conditions to which the BBD Buoy is expected to be subjected. In addition to this, further analysis using a more suitable software such as Ansys of the full model is recommended to obtain a clearer figure for the natural frequency of the structure in order to manage risk of a potential wave slam induced resonance.

B. Recommendations for Further Research

The software used for the FEA conducted in this study ruled out pursuing some of the objectives of the investigation. Modelling specialised reinforcements to the localised stress points was not possible using Robot Structural Analysis and the composite models represent more of a blueprint for the change in behaviour induced by the introduction of alternate materials to the design. Further analysis modelling the full-scale structure using a hi fidelity FEA software would provide a better representation of this behaviour, as well as precise results for the stress in the hull of the Buoy induced by wave impacts, particularly in localised stress points.

Specific suggestions for additional analysis include:

ACKNOWLEDGEMENT

The authors would like to acknowledge the data provided by Ocean Energy Ltd, Longitude Engineering through the Horizon Europe funded WEDUSEA project. The authors would like to acknowledge Autodesk for the use of ROBOT on academic license.

REFERENCES

- [1] W. Sheng, "Numerical modelling of the OE Wave Energy Converter," MaREI, Cork, 2019.
- [2] L. Fernández, "www.stastita.com," Statista, 9 February 2023. [Online]. Available: <https://www.statista.com/topics/4564/global-wind-energy/>. [Accessed 7 March 2023].
- [3] Precedence Research, "Wind Energy Market (By Location: Onshore and Offshore; By Application: Utility and Non-utility; By Component: Turbine, Support Structure, Electrical Infrastructure, Others) - Global Industry Analysis, Size, Share, Growth, Trends, Regional Outlook, and For," Precedence Research, Global, 2021.
- [4] IRENA, "IRENA Renewable Capacity Statistics 2022," The International Renewable Energy Agency, Abu Dhabi, 2022.
- [5] Fortune Business Insights, "Market Research Report," Fortune Business Insights, Global, 2020.

- [6] J. M. M. O. A. Bevin, "Structural Design Implications of Experimental Hull Pressure Analysis for a Floating Wave Energy Converter," 2022.
- [7] Longitude Engineering, "L032570 – WEDUSEA Ocean Energy Buoy Hull Design and Analysis Progression Update," ABL Group, 2023.
- [8] R. R. A. S. J. H. F. Boshell, "Unlocking the potential of Ocean Energy: from megawatts to gigawatts," *Energy Post*, 03 June 2020.
- [9] F. S. D. Janssen, "IRENA chief: Europe is 'the frontrunner' on tidal and wave energy," EURACTIV, 4 September 2020. [Online]. Available: <https://www.euractiv.com/section/energy/interview/irena-chief-europe-is-the-frontrunner-on-tidal-and-wave-energy/>. [Accessed 07 03 2023].
- [10] EMEC, "Grid-Connected Wave Test Site," EMEC, 2023. [Online]. Available: <https://www.emec.org.uk/facilities/wave-test-site/>. [Accessed 09 Mar 2023].
- [11] Deutsche Windtechnik, "Vestas V164-8.0," 2022. [Online]. Available: <https://en.wind-turbine-models.com/turbines/318-vestas-v164-8.0>. [Accessed Nov 2022].
- [12] Vestas, "Archi Expo," 2023. [Online]. Available: <https://pdf.archiexpo.com/pdf/vestas/vestas-v164-80-mw/88087-134417.html>. [Accessed Nov 2022].
- [13] Archi Expo, "Siemens Gamesa," 2023. [Online]. [Accessed Nov 2022].
- [14] University College Cork, "Sustainable Energy Ireland Energy R.D&D Programme," HMRC, Cork, 2005.
- [15] Engineering Toolbox, "Young's Modulus, Tensile Strength and Yield Strength Values for some Materials," Engineering Toolbox, 2003. [Online]. Available: https://www.engineeringtoolbox.com/young-modulus-d_417.html. [Accessed 22 March 2023].
- [16] DuPont, "Kevlar® Aramid Fiber Technical Guide," 2017. [Online]. Available: <https://www.dupont.com/content/dam/dupont/amer/us/en/safety/public/documents/en/>. [Accessed 22 March 2023].
- [17] N. Sonnichsen, "Worldwide capacity of marine energy 2009-2018," Statista, 2021.
- [18] C. O. J. Jose, "Methods for Analysing Wave Slamming Loads on Truss Structures Used in Offshore Wind Applications Based on Experimental Data," *International Journal of Offshore and Polar Engineering*, pp. 102-108, 2016.
- [19] T. Lewis CTO, Ocean Energy USA LLC., "Demonstration of the OE Buoy at US Navy's Wave Energy Test Site," U.S. Department of Energy, 2019.
- [20] Veritas, Rules for the Classification of Ships, Det Norske Veritas, 1998.
- [21] BBC, "Reasons for increase in demand for energy," BBC, 2023. [Online]. Available: <https://www.bbc.co.uk/bitesize/guides/zpmmmp3/revision/1>. [Accessed 03 March 2023].
- [22] International Energy Agency, "Electricity Market Report - July 2021," IEA, 2021.
- [23] World Material, "S235J0 Steel (EN 1.0114 Material) Datasheet, Properties, Meaning," 2023. [Online]. Available: <https://www.theworldmaterial.com/s235j0-steel-en-1-0114-material-datasheet/>. [Accessed 22 March 2023].